Computer Simulation of the Rough Lipopolysaccharide Membrane of *Pseudomonas aeruginosa*

Roberto D. Lins and T. P. Straatsma
Environmental Molecular Sciences Laboratory, Pacific Northwest National Laboratory, Richland, Washington 99352 USA

ABSTRACT Lipopolysaccharides (LPSs) form the major constituent of the outer membrane of Gram-negative bacteria, and are believed to play a key role in processes that govern microbial metal binding, microbial adsorption to mineral surfaces, and microbe-mediated oxidation/reduction reactions at the bacterial exterior surface. A computational modeling capability is being developed for the study of geochemical reactions at the outer bacterial envelope of Gram-negative bacteria. A molecular model for the rough LPS of *Pseudomonas aeruginosa* has been designed based on experimentally determined structural information. An electrostatic model was developed based on Hartree-Fock SCF calculations of the complete LPS molecule to obtain partial atomic charges. The exterior of the bacterial membrane was assembled by replication of a single LPS molecule and a single phospholipid molecule. Molecular dynamics simulations of the rough LPS membrane of *P. aeruginosa* were carried out and trajectories were analyzed for the energetic and structural factors that determine the role of LPS in processes at the cell surface.

INTRODUCTION

High concentrations of a variety of metal ion complexes are known to be harmful because of their toxic and genotoxic effects. Improper disposal of wastes has caused soil and water contamination, threatening a number of ecosystems around the world. Decontamination of soil and water via efficient biocatalysts is a promising cost-effective remediation strategy. Certain species of Gram-negative bacteria, e.g., *Pseudomonas aeruginosa*, are known for their ability to take up and/or reduce metal ions from the environment (Roden and Zachara, 1996; Truex et al., 1997; Gorby et al., 1998; Brooks et al., 1999; Roden and Urrutia, 1999; Urrutia et al., 1999; Texier et al., 1999, 2000). This ability, as well as the adhesion to mineral surfaces, has been reported to be mediated by the presence of lipopolysaccharides (LPSs), the main constituent of the outer bacterial membrane (Makin and Beveridge, 1996; DeFlaun et al., 1999; Langey and Beveridge, 1999). Understanding of these processes at a molecular level is essential for the design and development of bioremediation strategies, particularly in dealing with the technological difficulties in the transport of bacteria to the subsurface locations where they are needed. Molecular structures are available for LPS fragments of many Gram-negative bacteria. Complete structures for the entire LPS have been determined for *Escherichia coli* (Sengupta et al., 1995; Manca et al., 1996; Wang and Hollingsworth, 1996; Pristovsek and Kidric, 1999) and *P. aeruginosa* (Knirel et al., 1988; Rivera and McGroarty, 1989; Arsenault et al., 1991; Burrows et al., 1996; Sadovskaya et al., 1998, 2000). This study focuses on *P. aeruginosa*, a Gram-negative bacterium that has been reported to reduce chlorides, sulfates, and nitrates, as well to bind a variety of metal ions, such as Na, Al, Ca, Fe, La, Eu, Yb, and U (Langey and Beveridge, 1999). It is naturally found in sediments, and adhesion data for glass and polystyrene are available (Lyklema et al., 1989).

Three distinct regions can be identified in LPS: the lipid *A*, the core region, and the O-specific chain. In *P. aeruginosa*, two types of O-specific chains have been identified (Burrows and Lam, 1999). The presence or absence and type of O-specific chain seem to be environmentally controlled and provides a means of classification of the LPS membrane: A+B+, A−B−, A+B−, and A−B+. The classification A−B− represents the so-called rough LPS. The *P. aeruginosa* A-band LPS is a neutral homopolymer of $[\text{-}\alpha\text{-D-rhamnose-}]_3$, whereas the B-band repeating unit is a heteropolymer formed by uronic acid derivatives and rare sugars such as pseudaminic acid. Although the B-band consists of saccharide units rich in carboxyl groups, the rough LPS has been identified to be the most negatively charged membrane followed by the A−B+ type. The saccharide sequence in the core region is always present in the LPS molecule, and structurally identical for all strains of the bacterium. Lipid *A* consists of two glucosamine-phosphate moieties bound to the lipid chains that can vary in length and number depending on the bacterium strain. Although the transport of ions across the bacterial membrane is likely to occur through protein channels, the type of O-antigen chain expressed by the LPS membrane has been shown to determine uptake by the membrane (Langey and Beveridge, 1999). Ions such as Cu, Fe, La, Eu, and U were identified to bind in the cell wall of *P. aeruginosa* (Langey and Beveridge, 1999; Texier et al., 2000) and this suggests the availability of metallic ion binding sites in the core region (Langey and Beveridge, 1999). Phosphate and carboxyl groups of the core region of the LPS were found to play the major role in the metal ion binding (Texier et al., 2000).

Received for publication 16 January 2001 and in final form 11 May 2001.
Address reprint requests to Dr. T. P. Straatsma, Environmental Molecular Sciences Laboratory, Pacific Northwest National Laboratory, Richland, WA 99352, USA. Tel.: 509-375-2802; Fax: 509-375-6631; E-mail: tp_straatsma@pnl.gov

0006-3495/01/08/1037/10 $2.00

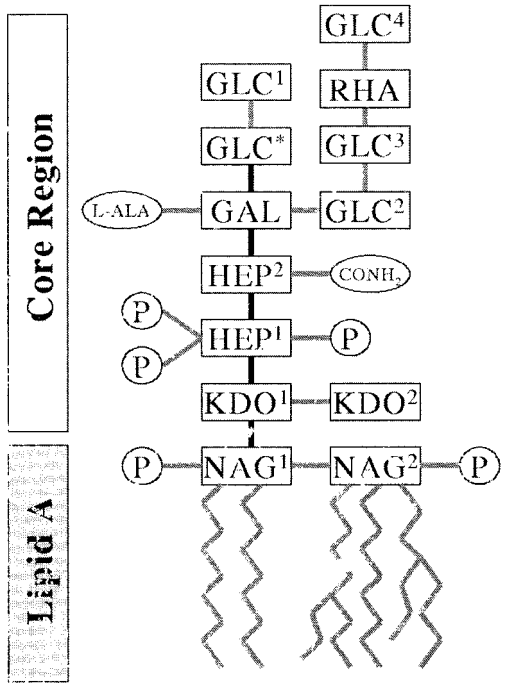

FIGURE 1 Schematic structure of the rough LPS of *Pseudomonas aeruginosa* strain PA01. NAG, *N*-acetylglucosamine; KDO, 2-keto-3-deoxy-D-mannooctonic acid; P, phosphate group; HEP, heptose; GAL, galactose; ALA, alanine; GLC, glycose; RHA, rhamnose.

To understand the LPS mediated uptake and transport of ions from the environment to the cellular membrane a molecular model was developed for the rough LPS membrane of *P. aeruginosa*. Because experimental and theoretical data of the three-dimensional structure of the LPS membrane are unavailable, a molecular model for the LPS membrane was built using models of single molecules of LPS and phospholipid chain. Computational chemistry methods were used to complete the set of force field parameters needed for the molecular simulations of the system. The resulting molecular trajectories were analyzed for its general structural and dynamical behavior, conformational changes, ion, solvent and charge distributions, and the electrostatic potential along and across the LPS membrane.

METHODS

Molecular modeling of a single LPS

A three-dimensional molecular model of a single rough LPS (lipid *A* and core region) of *P. aeruginosa* PA01 was generated based on experimentally available sequence data for the LPS monomer (Sadovskaya et al., 1998; Fig. 1). The structure was straightened to its maximum length through the application of a number of restraint potentials. Six Ca^{2+} and one Na^{+} ions were placed near the structure to neutralize the original charge (-13 *e*) of the LPS unit. This geometry was optimized using 100 steps of steepest descent energy minimization. Hartree-Fock SCF calculations of the complete optimized molecule (474 LPS atoms and 7 counter ions) at the 6–31G* level (4309 basis functions) and restrained electrostatic potential (Bayly et al., 1993) fitting calculations were carried out using NWChem (Pacific Northwest National Laboratory, Richland, WA; Harrison et al., 2000) to obtain partial atomic charges. The same procedure was used to obtain partial atomic charges for a phospholipid molecule. These charges were used in combination with the AMBER95 (Cornell et al., 1995) and GLYCAM_93 (Woods et al., 1995) force field parameters in subsequent molecular dynamics simulations.

Building the LPS membrane

A single rough LPS model was replicated in space, generating a 4×4 LPS arrangement with a distance of at least 1.0 nm between any pair of atoms from different LPS molecules to provide sufficient space for rotation of each molecule during the equilibration of the membrane. Similarly, a 40-molecule phosphatidylethanolamine (PE) membrane was assembled at the bottom of the 16 LPS molecules to complete the lipid matrix of the outer membrane of the Gram-negative bacterium *P. aeruginosa*. All subsequent simulations were carried out under periodic boundary conditions, such that the membrane consists of a periodic layer of LPS molecules exposed to an exterior aqueous environment and a PE layer also exposed to water, representing the periplasmic space. An electrostatic grid calculation was performed to determine the positions of 104 Ca^{2+} ions to neutralize the system. To ensure the integrity of the membrane, a restraining potential was applied, during the equilibration phase, to the *N*-acetylglucosamine (NAG) residues of all LPS molecules to keep these groups in the plane of the membrane. A similar restraining potential was also applied to the phosphate groups of the phospholipid molecules. Additional restraining potentials were applied to all lipid chains to keep them aligned in the direction normal to the plane of the membrane.

Through application of high-pressure anisotropic coordinate scaling (1.025×10^8 Pa) and incremental increase of the temperature by scaling of the atomic velocities, the physical gaps between each subunit were gradually eliminated. A 1.8-nm cutoff was used during the 200-ps molecular dynamics (MD) simulation under periodic boundary conditions. To avoid interactions between the saccharide units on the top of the membrane and periodic images of its bottom lipids, a large box perpendicular to the membrane was used and no pressure scaling was applied in that dimension. The temperature was raised from 0 to 300K in increments of 50K each 20 ps of MD simulation using a 1-fs time step. The resulting structure was solvated using periodic boundary conditions such that a layer of water was added on both sides of the membrane. The SPC/E water model was used (Berendsen et al., 1987). The final system

consisted of 10,384 LPS/lipid atoms, 104 Ca^{2+} ions and 3080 water molecules. The dimensions of the simulation volume were $3.53 \times 4.82 \times 11.16$ nm. All MD simulations were carried out using NWChem.

The solvent, on top and at the bottom of the fixed solute (LPS, lipids, and ions), was energy-minimized using 200 steps of steepest descent, followed by 200 conjugate gradient steps. Equilibration of the solvent, with the solute atoms fixed, was performed for 20 ps at 300 K. All solute atoms were minimized, keeping the solvent coordinates fixed, after which the whole system was simulated for 80 ps at 300 K using a 2-fs time step. An additional 100 ps MD simulation at 300 K, 1.025×10^5 Pa, using a 2-fs time step, was performed in which the restraint potentials were removed, with exception of a weak restraint potential keeping the PE head groups in the plane of the membrane. This restraint potential was used during the entire production.

Molecular dynamics simulation

MD simulations in the isothermal-isobaric ensemble were carried out for 1 ns using the leapfrog algorithm with a 2-fs time step (Hockney, 1970). The temperature was maintained at 300 K by weak coupling to a heat bath with relaxation times for solvent and solute of 0.4 and 0.1 ps, respectively. The pressure of the system was maintained at 1.025×10^5 Pa by anisotropic coordinate scaling with a relaxation time of 0.4 ps. SHAKE constraints (Ryckaert et al., 1977) with a tolerance of 10^{-4} nm were applied to all bonds involving a hydrogen atom.

Electrostatic potential calculation

The electrostatic potential at a given coordinate in space x, $\phi(x)$, is defined as the work necessary to bring unit positive charge from infinity to x. The electrostatic interaction energy between a point charge q located at x and the molecule is equal to $q\phi(x)$. The electrostatic potential across the LPS membrane was calculated from the partial atomic charges used in the simulations. In these calculations, edge-related artifacts were avoided by using periodic boundary conditions. The grid was extended up to 1.0 nm beyond the solute atoms in the transmembrane axis and the water molecules removed for the electrostatic potential calculation. Ten grid points per nm and a 2.0 nm cutoff for the periodic space only were used.

RESULTS AND DISCUSSION

Dynamical equilibrium

After 200 ps of equilibration, the simulation was run for 1 ns. During this simulation, no systematic drift was observed in the temperatures of solute and solvent, the potential energy of the system, or individual contributions to the potential energy from nonbonded intrasolute and solute-solvent interactions, indicating that the system had attained equilibrium. The root mean square deviations (RMSD) from the initial, equilibrated structures were evaluated for each of the 16 LPS molecules (Fig. 2, *a* and *b*), as well as for the entire membrane. RMSDs <0.2 nm were found for 14 of the 16 LPS molecules throughout the simulation. The two LPS molecules 14 and 16 showed a RMS deviation of 0.5 and 0.4 nm, respectively. (Fig. 2 *b*) The RMSD for the entire LPS membrane was observed to be constant at approximately 0.2 nm. It suggests that the membrane has reached structural equilibrium and is not affected by the larger flexibility of LPS molecules 14 and 16. Inspection of the trajectory revealed that the motions were primarily confined to a specific outer core region of these molecules, as will be discussed in more detail.

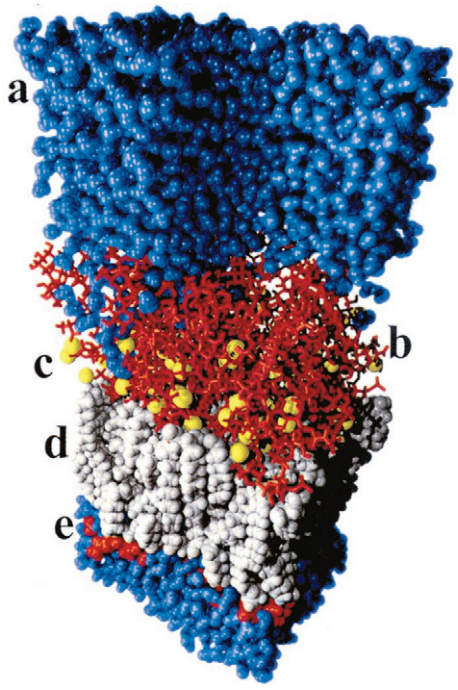

FIGURE 2 Molecular model of the rough LPS membrane of *Pseudomonas aeruginosa*, showing the water layer (*a*) of which a cross-section cut was made to display the top of the sugars (*b*). The yellow spheres represent Ca^{2+} ions (*c*). Also shown is the phospholipid layer (*d*) polar head groups (*e*) immersed in water.

Conformational analysis of the LPS membrane

Once energetically and structurally equilibrated, the double lipid matrix exhibited a gel-type structural arrangement, as expected at the temperature of the simulation. A representation of this structure is given in Fig. 3. The LPS membrane initially compressed but no significant volume fluctuations were observed in the last 500-ps interval. A measure of the lipid layer density is the surface area per single lipid unit.

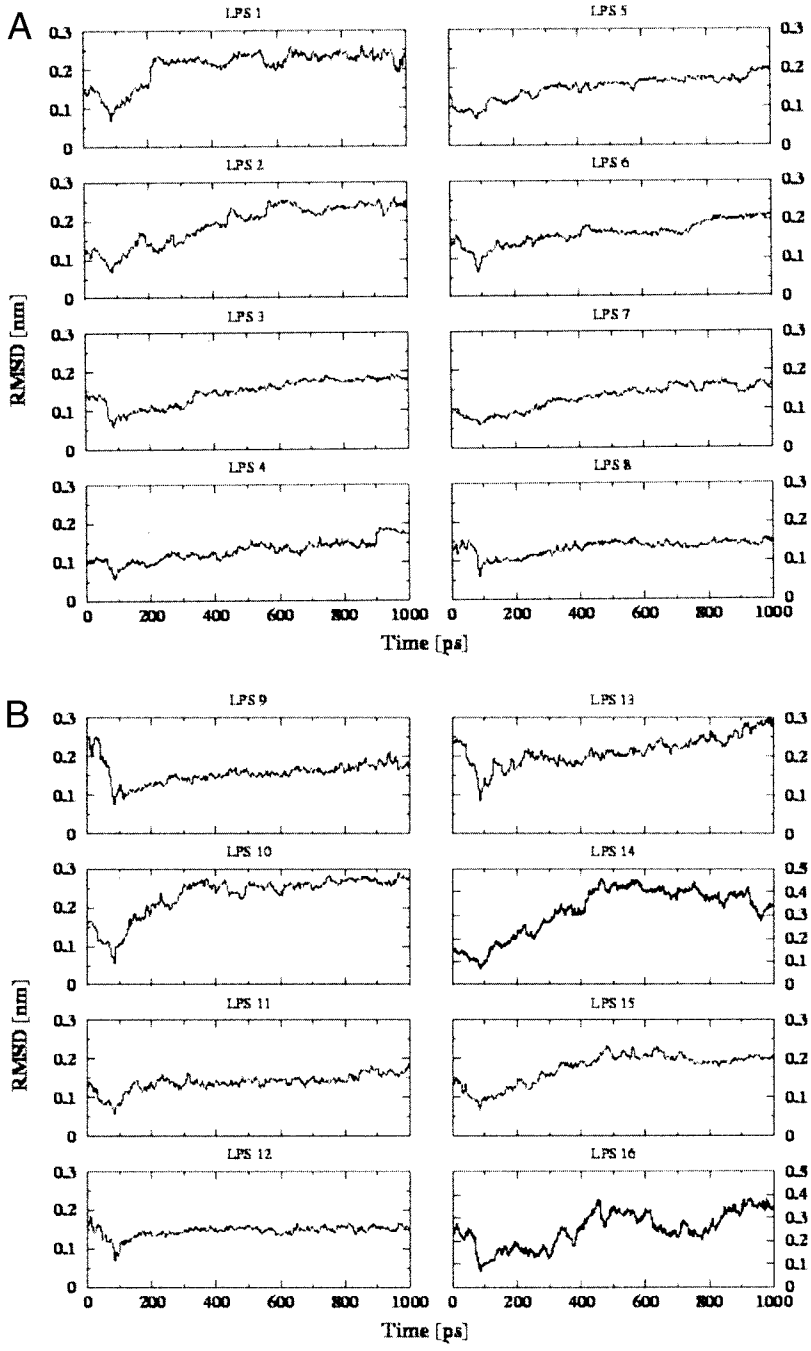

FIGURE 3 RMSD for each of the 16 LPS molecules. (*a*) RMSD for LPS units 1–8. (*b*) RMSD for LPS units 9–16.

For the final structure of the simulation, this area is 0.403 nm^2, in very good agreement with the experimental value for the same area in a double PE membrane in the gel state, reported to be 0.41 nm^2 (McIntosh and Simon, 1986).

The good agreement for this property strongly depends on the atomic charge model used (Schuler, 2000), which for our simulations was determined using the procedure with which the AMBER95 force field parameters were determined.

The flexibility of each of the 16 LPS molecules in the membrane was individually analyzed. For the conformational analysis, an LPS "backbone" was defined as the trace of torsion angles through the nonvariable saccharide monomers starting at the lipid *A* to the top of the LPS. The saccharide monomers involved are those connected by the dark lines in Fig. 1. Torsion angles involving atoms belonging to the same saccharide ring were not taken into account in this analysis because they do not change the overall

conformation. The number of variable torsion angles linking the 6 saccharides (NAG^1, KDO^1, HEP^1, HEP^2, GAL, and GLC*) is 7 for each of the 16 LPS molecules. Two potentially flexible torsions link NAG^1 and KDO^1 as well as GAL and GLC*, whereas a single bond connects each pair of internal saccharides.

The behavior of the seven torsions in each LPS was analyzed and compared. Although, in some cases, more than one preferential conformation was identified for certain torsion angles in different LPS units, little flexibility was observed for a specific torsion. Significant conformational changes were observed for only 15 of 112 dihedral angles analyzed in the 16 LPS units. The flexible points involved the dihedral angles linking the lipid A to the core region (low amplitude) and the linkage between GAL and GLC*, where 4 of 16 GAL-GLC* dihedral pairs did not present any well defined conformation. These are the only linkages that are formed by two dihedral angles. Some degree of flexibility between the lipid *A* and the core region of the LPS is to be expected; it allows an easier rearrangement of the core region of different LPS units on ion or solvent exchange without perturbing the structure of the double lipid matrix. However, the high flexibility of one specific region in the interior of the core region can only be understood by investigation of the attachment location of the O-specific chain. Recent studies of the structure of the LPS of *P. aeruginosa* show that the B-band attaches specifically to the GLC* residue (Sadovskaya et al., 2000; Fig. 1). This is in agreement with observations from a previous MD simulation of a single LPS molecule consisting of a lipid *A* from *E. coli* and a core region and O-specific chain from *Salmonella typhimurium*. Kastowsky et al. (1992) identified the O-specific chain as the most flexible part of the LPS, whereas the lipid *A* and core region presented a well defined conformation. Note that only about one-fourth of the B-band attachment sites showed significant flexibility in the present simulation. However, only 6 to 8% of the LPS units in a nonrough strain carry an O-specific chain. Therefore, not all GAL-GLC* connection points in the LPS membrane matrix need to have the same degree of flexibility. The B-band is exposed to the environment and can be very long, up to 60-mer (Lam et al., 1992; Sadovskaya et al., 2000). The presence or absence of the O-specific chain has been shown to be environmentally controlled (Makin and Beveridge, 1996).

Ca^{2+} ion distribution

Visual inspection indicated the Ca^{2+} ions to be predominantly hexacoordinated, giving a total of 624 possible coordination sites for Ca^{2+} ions; LPS atoms occupied 472 of these sites during the entire trajectory. Therefore, about 75% of the Ca^{2+} coordination sites bind LPS atoms, whereas 25% of the sites are available to interact with other molecules, such as water. Because an average of 50 water molecules are found inside the LPS at any given time, this

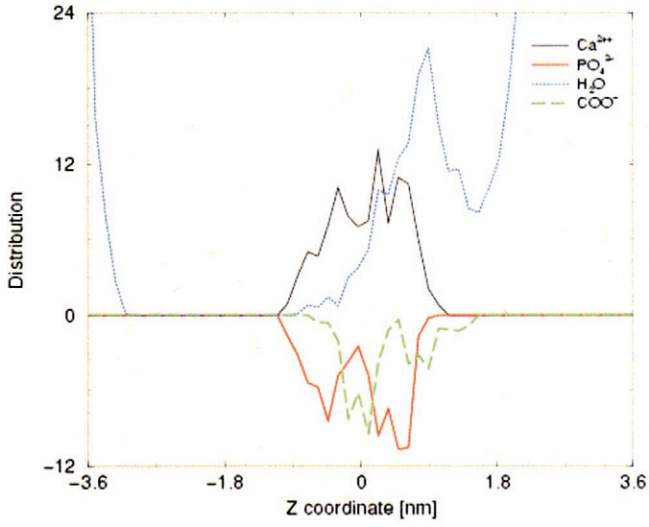

FIGURE 4 Charged groups distribution along the transmembrane axis of the LPS membrane. The plots for PO_4^{2-} and COO^- are inverted for clarity. Distributions shown are for the last 500 ps of the simulation.

suggests that an ion does not have to be completely desolvated to be taken up by the membrane. Most of the Ca^{2+} ions are confined in a thin area (≈2 nm) in the inner core region of the LPS membrane (≈10 nm) and interact mainly with the phosphorylated sugars. Fig. 4 shows a detailed distribution of Ca^{2+} ions and negatively charged LPS groups along the membrane. Whereas the distribution of phosphate groups is spatially split into two regions, the Ca^{2+} distribution is fairly uniform, because of the positioning of the carboxyl groups filling the gap between the phosphate distributions. The average contribution to Ca^{2+} binding from each sugar residue in the LPS membrane is shown in Table 1. All Ca^{2+} ions were found to interact with phosphate groups. On average, a Ca^{2+} ion interacts with three phosphates. This corresponds to 50% of the total number of Ca^{2+} ion coordination sites. Of the sites, 15% coordinate carboxyl groups, and 10% interact with hydroxyl groups. A total of approximately 300 water molecules were exchanged between the membrane and the medium during the 1-ns MD simulation. The LPS membrane immobilizes the Ca^{2+} ion very effectively. Although some mobility was observed, none of the ions diffused to the aqueous environment. The important role of ions in maintaining the integrity of the LPS membrane has been previously addressed (Kotra et al., 1999).

Because the phosphate groups are shown to play the most significant role in cation binding, the conformational distribution of the ions in the two phosphate-rich regions was analyzed. The phosphate groups bound to the NAG sugars form the first region, from the bottom to the top, and are characterized by two PO_4^{2-} groups/LPS. The other phosphate-rich region is formed by the HEP^2 monomers, each contributing three PO_4^{2-} groups. These two regions show

TABLE 1 Average contribution to Ca binding

LPS residue	Group	Number of functional groups per residue contributing to Ca^{2+} binding
$NAG^{1,2}$	•OH	7
KDO^{1}	•OH	13
	$•COO^{-}$	32
KDO^{1} total		[45]
KDO^{2}	•OH	21
	$•COO^{-}$	34
KDO^{2} total		[55]
P	$•PO_4^{[2-]}$	312
HEP^{1}	•OH	7.5
HEP^{2}	•OH	10.5
GAL	•OH	3
	$•COO^{-}$	28
GAL total		[31]
GLC*	•OH	3
GLC^{14-}	•OH	0.6
RHA	•OH	0.4
Total		472

Average functional group contribution to Ca^{2+} binding per residue. Binding is based on contact between the ion and the functional group atoms. Numbers in square brackets are total numbers of ion interactions for all functional groups in the indicated residue.

substantial structural differences. Fig. 5, *a* and *b* show a cross-section from a representative snapshot of the LPS membrane for these areas. Fig. 5 *a* displays clusters of four phosphate groups, where each group branches out from a different NAG residue. In contrast, Fig. 5 *b* does not exhibit any recognizable structural pattern. The Ca^{2+} ion arrangement seems to be more structurally defined in the lower region than in the top one. The presence of a structural pattern suggests the lower portion of the LPS core to be less mobile. Despite of the observed structural pattern no correlation was found between binding energy and the spatial distribution of the Ca^{2+} ions in the LPS membrane.

To study the mobility of the different regions, an essential dynamics (ED) analyses (Amadei et al., 1993; van Alten et al., 1997) were carried out for the Ca^{2+} ions and for the two most flexible LPS units, numbers 14 and 16 (Fig. 2, *a* and *b*). ED analysis describes the atomic motions with respect to an average structure in terms of a set of orthogonal vectors obtained by diagonalization of the covariance matrix of the atomic fluctuations. The most persistent motions are represented by the eigenvectors with largest average square displacements, i.e., the eigenvalues. Consequently, the corresponding eigenvectors characterize the largest positional deviations. The ED analysis technique has been successfully applied in a number of protein simulation studies to determine the most mobile regions and their corresponding relative amplitudes amplitude (van Alten et al., 1997; Weber et al., 1998; Lins et al., 1999a, b).

RMSD calculations and ED analysis were carried out to determine the mobility of the Ca^{2+} ions. The calculated average RMSD of 0.08 nm and the absence of large motions as revealed by the ED analysis of the entire trajectory are an indication of the low flexibility of the membrane in the inner core regions, where the Ca^{2+} ions are found. Although the solvent exposed region is flexible, as described in "Internal flexibility of the LPS units," the structure of the inner core region is well defined. This raises the question of the inner core region being trapped in one of many possible structures. Because of the strong electrostatic interactions in this region, the expected high-energy barriers between the different inner core structures will cause transitions between them to take place on a much longer timescale than the length of the molecular dynamics simulation.

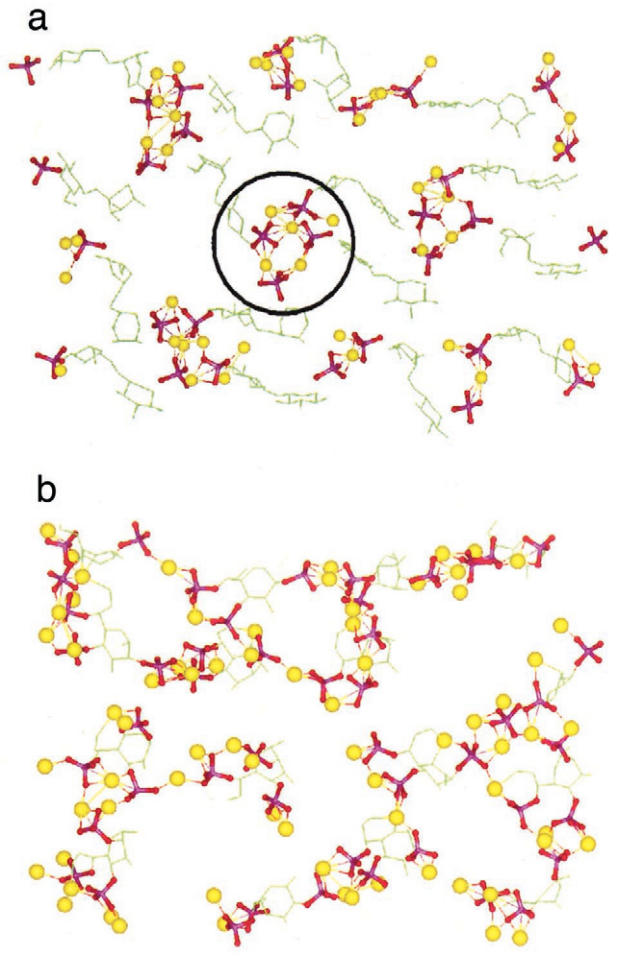

FIGURE 5 Spatial distribution of the Ca^{2+} ions in lipid *A*/inner core (*a*) and outer core regions (*b*) of the LPS membrane. Distributions are shown for the final structure obtained from the 1-ns MD simulation.

Internal flexibility of the LPS units

Time-frame ED analysis was performed for the individual LPS units over the last 500 ps of the MD trajectory. Each frame of the trajectory was superimposed on a reference

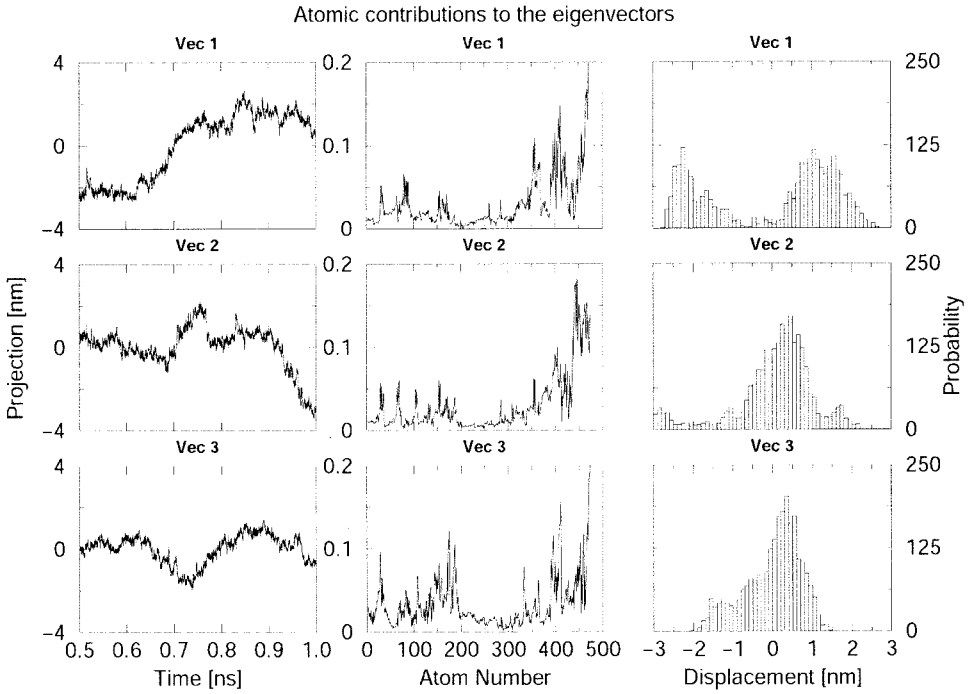

FIGURE 6 Essential dynamics analysis plots for LPS molecule 14. Frames at 10-ps intervals during the last 500 ps of the MD simulation were used to generate the presented data.

structure eliminating the effects from overall translational and rotational motions. For the ED analysis, the average structure was used as reference and only heavy atoms were taken into account.

The relative internal motions for the two most flexible LPS units 14 and 16 were investigated (Fig. 2 *a* and *b*) and exhibited a common pattern. Fig. 6 illustrates the projections of the trajectories onto the first three eigenvectors (*left*), the atomic contributions (*center*), and the probability distributions from these projections (*right*) for LPS unit 14. The inner core region exhibits a low persistent motion (atoms 176–339), compared to the lipid *A* (atoms 1–175) and especially to the outer core (atoms 340–474). Note that the first eigenvector, representing the lowest frequency mode, shows two main conformational states. Eigenvectors 2 and 3 present a one conformational state with a Gaussian-like distribution (Fig. 6).

Structural analysis of the maximum and minimum projections onto the first eigenvector of LPS units 14 and 16 shows the largest positional deviations to occur in the GLC* conformation. This is the result of the combined flexibility of the two dihedrals linking GAL and GLC*. It is represented by the largest eigenvalue, and therefore constitutes the most persistent motion exhibited by the LPS units 14 and 16. By acting as a "hinge" point in the LPS unit, the flexibility on GLC* minimizes the thermodynamic cost of attaching/detaching the O-specific chain upon environmental demands.

Electrostatic signature

Gram-negative bacteria, such as *P. aeruginosa*, have the ability to adsorb to mineral surfaces (Makin and Beveridge, 1996; DeFlaun et al., 1999). Important for this interaction are the electrostatic properties of the outer membrane, i.e., the LPS membrane surface (DeFlaun et al., 1999). Understanding and characterizing the electrostatic properties of the LPS membrane is, therefore, important for the study of the potential use of these organisms for environmental remediation.

The electrostatic potential was calculated for several structures from the MD trajectories, showing well-defined separation of negative and positive charge in the membrane (Fig. 7 *a*). Large, negatively charged patches on the membrane surface can be seen in the Fig. 7 *a*, whereas a positive region is found in the LPS inner core. This charge distribution is a result of the distribution of the Ca^{2+} ions across the membrane, which are spatially restricted to the inner core. This finding agrees qualitatively with and contributes to the understanding of the experimentally reported negative potential of the rough LPS membrane surface. The rough LPS (A−B−) has a highly electronegative surface compared with strains that contain any form of O-specific chain (Makin and Beveridge, 1996). Secondly, these negative patches are found to change shape frequently in the surface of the LPS membrane. Changes in these membrane patches were found to occur in the fs timescale (Fig. 7 *b*). This

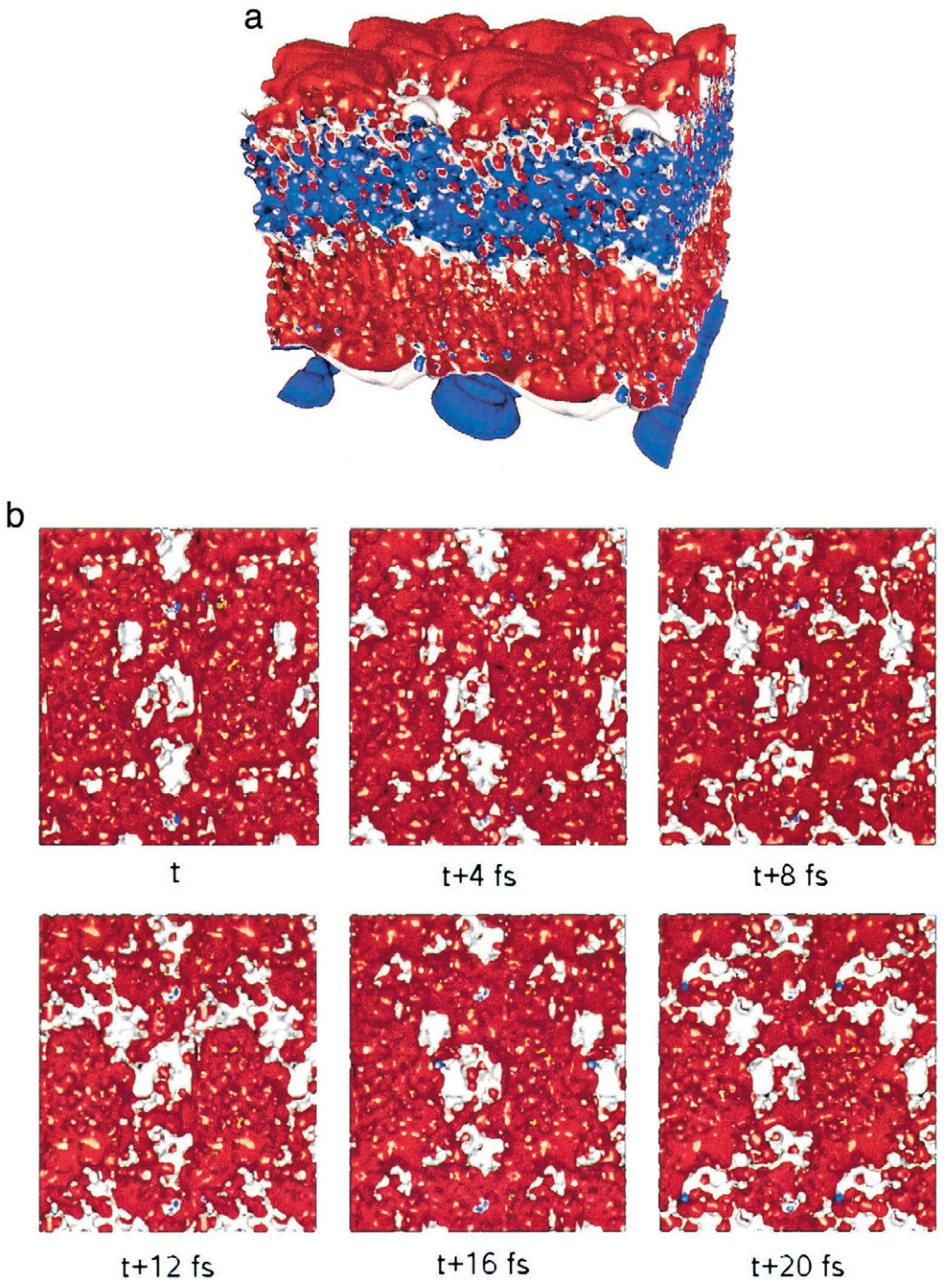

FIGURE 7 Electrostatic potential isocontours at −150 mV (*red*), 0 mV (*white*), and +150 mV (*blue*) of the rough LPS membrane of *Pseudomonas aeruginosa*. (*a*) Side view of the contours as in the final structure obtained from the 1-ns MD simulation. (*b*) Dynamic changes exhibited in the electrostatic potential by a series of snapshots taken 4 fs apart in the last 200 ps of the MD simulation.

suggests that the membrane has a high adaptability for interactions between the LPS membrane of *P. aeruginosa* and a variety of structurally different, positively charged mineral surfaces, as well as approaching cations.

Studying the role of porins in *Paracoccus denitrificans*, Wiese et al. (1994) reported that voltages in the order of 100 mV or greater had to be applied to the LPS/phospholipid bilayers to affect channel gating behavior of porins. The depolarization of a membrane depends on its composition. Using a carrier-ion complex, Seydel et al. (1992) reported values for the voltage across the rough LPS membrane and determined the potential difference between the phospholipid and the lipopolysaccharide to be −85 mV. Based on the molecular and electrostatic models used in this study,

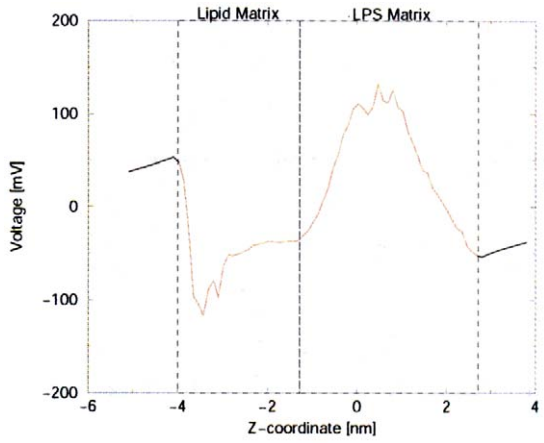

FIGURE 8 Calculated potential difference in the transmembrane axis of the LPS membrane. Values are from 10-ps interval averages throughout the last 500 ps of the MD simulation. Plot values for the region within the lipid and LPS matrices are shown in gray.

this difference, from the 10-ps interval average taken over the last 500 ps of MD simulation, is found to be ≈ -100 mV (Fig. 8) for *P. aeruginosa*.

CONCLUSIONS

Results are presented here for the analysis of molecular dynamics simulations of the rough LPS membrane of *P. aeruginosa.* The membrane displayed little flexibility as a whole. Ions, needed to stabilize the membrane structure because of the huge negative charge in the inner core, are uniformly distributed across a small region in the inner core, and complement the distribution of the negatively charged functional groups. A well defined structural arrangement is found for the Ca^{2+} ions that interact with inner core phosphate groups. A highly negative electrostatic potential surface on the LPS membrane is found, which corresponds very well with experimentally determined transmembrane potentials. The fast dynamics of the patches of negative charge on the surface and the large flexibility of the B-band insertion points suggest that the LPS membrane of *P. aeruginosa* is able to adapt to approaching environmental ions or mineral surfaces. Further studies on the energetics, ionic exchange properties, and mineral surface adhesion as a function of LPS membrane composition are needed and some are underway.

We thank Drs. Andy R. Felmy, David A. Dixon, and Lukas Schuler for many useful discussions. The Geosciences Research Program of the U.S. Department of Energy, Office of Basic Energy Sciences supported this project. Computing resources were available through a Computational Grand Challenge Application grant from the Molecular Science Computing Facility at the Environmental Molecular Sciences Laboratory. The NWChem 4.0 computational chemistry package for massively parallel computers used in this study was developed by the High Performance Computational Chemistry group, Environmental Molecular Sciences Laboratory, Pacific Northwest National Laboratory. Battelle Memorial Institute operates Pacific Northwest National Laboratory for the U.S. Department of Energy.

REFERENCES

Amadei, A., A. B. M. Linssen, and H. J. C. Berendsen. 1993. Essential dynamics of proteins. *Proteins* 17:412–425.

Arsenault, T. L., D. W. Hughes, D. B. MacLean, W. A. Szarek, A. M. B. Kropinski, and J. S. Lam. 1991. Structural studies on the polysaccharide portion of "A-band" lipopolysaccharide from a mutant (AK1401) of *Pseudomonas aeruginosa* strain PAO1. *Can. J. Chem.* 69:1273–1280.

Bayly, C. I., P. Cieplak, W. D. Cornell, and P. A. Kollman. 1993. A well-behaved electrostatic potential based method using charge restraints for deriving atomic charges: the RESP model. *J. Phys. Chem.* 97:10269–10280.

Berendsen, H. J. C., J. R. Grigera, and T. P. Straatsma. 1987. The missing term in effective pair potential. *J. Phys. Chem.* 91:6269–6271.

Brooks, S. C., S. L. Carroll, and P. M. Jardine. 1999. Sustained bacterial reduction of $Co^{III}EDTA^-$ in the presence of competing geochemical oxidation during dynamic flow. *Environ. Sci. Technol.* 33:3002–3011.

Burrows, L. L., D. F. Charter, and J. S. Lam. 1996. Molecular characterization of the *Pseudomonas aeruginosa* serotype O5 (PAO1) B-band lipopolysaccharide gene cluster. *Mol. Microbiol.* 22:481–495.

Burrows, L. L., and J. S. Lam. 1999. Effect of *wzx (rfbX)* mutations on A-band and B-band lipopolysaccharide biosynthesis in *Pseudomonas aeruginosa* O5. *J. Bacteriol.* 181:973–980.

Cornell, W. D., P. Cieplak, C. I. Bayly, I. R. Gould, K. M. Merz, D. M. Ferguson, D. C. Spellmeyer, T. Fox, J. W. Caldwell, and P. A. Kollman. 1995. A second generation force field for the simulation of proteins, nucleic acids and organic molecules. *J. Am. Chem. Soc.* 177:5179–5197.

DeFlaun, M. F., S. R. Oppenheimer, S. Streger, C. W. Condee, and M. Fletcher. 1999. Alterations in adhesion, transport, and membrane characteristics in an adhesion-deficient pseudomonad. *Appl. Environ. Microbiol.* 65:759–765.

Gorby, Y. A., F. Cacavo, and H. Bolton. 1998. Microbial reduction of $Cobalt^{III}EDTA^-$ in the presence of manganese(IV) oxide. *Environ. Sci. Technol.* 32:244–250.

Kastowsky, M., T. Gutberlet, and H. Bradaczek. 1992. Molecular modelling of the three-dimensional structure and conformational flexibility of bacterial lipopolysaccharide. *J. Bacteriol.* 174:4798–4806.

Harrison, R. J., J. A. Nichols, T. P. Straatsma, M. Dupuis, E. J. Bylaska, G. I. Fann, T. L. Windus, E. Apra, J. Anchell, D. Bernholdt, P. Borowski, T. Clark, D. Clerc, H. Dachsel, B. de Jong, M. Deegan, K. Dyall, D. Elwood, H. Früchtl, E. Glendenning, M. Gutowski, A. Hess, J. Jaffe, B. Johnson, J. Ju, R. Kendall, R. Kobayashi, R. Kutteh, Z. Lin, R. Littlefield, X. Long, B. Meng, J. Nieplocha, S. Niu, M. Rosing, G. Sandrone, M. Stave, H. Taylor, G. Thomas, J. van Lenthe, K. Wolinski, A. Wong, and Z. Zhang. 2000. *NWChem, A Computational Chemistry Package for Parallel Computers, Version 4.0,* High Performance Computational Chemistry Group, Pacific Northwest National Laboratory, Richland.

Hockney, R. W. 1970. The potential calculation and some applications. *Methods Comput. Phys.* 9:136–211.

Knirel, Y. A., E. V. Vinogradov, N. A. Kocharova, N. A. Paramonov, N. K. Kochetkov, B. A. Dmitriev, E. S. Stanislavsky, and B. Lányi. 1988. The structure of O-specific polysaccharides and serological classification of *Pseudomonas aeruginosa. Acta Microbiol. Hungarica* 35:3–24.

Kotra, L. P., D. Golemi, N. A. Amro, G.-Y. Liu, and S. Mobashery. 1999. Dynamics of the lipopolysaccharide assembly on the surface of *Escherichia coli. J. Am. Chem. Soc.* 121:8707–8711.

Lam, J. S., L. L. Graham, J. Lightfoot, T. Dasgupta, and T. J. Beveridge. 1992. Ultrastructural examination of the lipopolysaccharide of *Pseudomonas aeruginosa* strains and their isogenic rough mutants by freeze-substitution. *J. Bacteriol.* 174:7159–7167.

Langey, S., and T. J. Beveridge. 1999. Effect of O-side-chain-lipopolysacchaide chemistry on metal binding. *Appl. Environ. Microbiol.* 65:489–498.

Lins, R. D., J. M. Briggs, T. P. Straatsma, H. A. Carlson, J. Greenwald, S. Choe, and J. A. McCammon. 1999a. Molecular dynamics studies on the HIV-1 integrase catalytic domain. *Biophys. J.* 76:2999–3011.

Lins, R. D., T. P. Straatsma, and J. M. Briggs. 1999b. Similarities in the HIV-1 and ASV integrase active sites upon metal cofactor binding. *Biopolymers* 53:308–315.

Lyklema, J., W. Norde, M. C. M. van Loosdrecht, and A. J. B. Zehnder. 1989. Adhesion of bacteria to polystyrene surfaces. *Colloid Surface.* 39:175–187.

Makin, S. A., and T. J. Beveridge. 1996. The influence of A-band and B-band lipopolysaccharide on the surface characteristics and adhesion of *Pseudomonas aeruginosa* to surfaces. *Microbiology* 142:299–307.

Manca, M. C., A. Weintraub, and G. Widmalm. 1996. Structural studies of the *Escherichia coli* $O_2$6 O-antigen polysaccharide. *Carbohydr. Res.* 281:155–160.

McIntosh, T. J., and S. A. Simon. 1986. Area per molecule and distribution of water in fully hydrated dilauroylphosphatidylethanolamine bilayers. *Biochemistry* 25:4948–4952.

Pristovsek, P., and J. Kidric. 1999. Solution structure of polymyxins B and E and effect of binding to lipopolysaccharide: an NMR and molecular modeling study. *J. Med. Chem.* 42:4604–4613.

Rivera, M., and E. J. McGroarty. 1989. Analysis of a common-antigen lipopolysaccharide from *Pseudomonas aeruginosa. J. Bacteriology.* 171:2244–2248.

Roden, E. E., and M. M. Urrutia. 1999. Ferrous iron removal promotes microbial reduction of crystalline iron(III) oxides. *Environ. Sci. Technol.* 33:1847–1853.

Roden, E. E., and J. M. Zachara. 1996. Microbial reduction of crystalline iron(III) oxides: influence of oxide surface area and potential for cell growth. *Environ. Sci. Technol.* 30:1618–1628.

Ryckaert, J. P., G. Ciccotti, and H. J. C. Berendsen. 1977. Numerical integration of the cartesian equations of motion of a system with constraints: molecular dynamics of *N*-alkanes. *J. Comp. Phys.* 23: 327–341.

Sadovskaya, I., J.-R. Brisson, J. S. Lam, J. C. Richards, and E. Altman. 1998. Structural elucidation of the lipopolysaccharide core regions of the wild-type strain PAO1 and O-chain-deficient mutant strains AK1401 and AK1012 from *Pseudomonas aeruginosa* serotype O5. *Eur. J. Biochem.* 255:673–684.

Sadovskaya, I., J.-R. Brisson, P. Thibault, J. C. Richards, J. S. Lam, and E. Altman. 2000. Structural characterization of the outer core and the O-chain linkage region of lipopolysaccharide from *Pseudomonas aeruginosa* serotype O5. *Eur. J. Biochem.* 267:1640–1650.

Schuler, L. D. 2000. Molecular dynamics simulation of aggregates of lipids: development of force field parameters and application to membranes and micelles. Ph.D. thesis, Diss. *ETH Nr.* 14009.

Sengupta, P., T. Bhattacharyya, A. S. Shashkov, H. Kochanowski, and S. Basu. 1995. Structure of the O-specific side chain of the *Escherichia coli* O128 lipopolysaccharide. *Carbohydr. Res.* 277:283–290.

Seydel, U., W. Eberstein, G. Schroder, and K. Brandenburg. 1992. Electrostatic potential barrier in asymmetric planar lipopolysaccharide/phospholipid bilayers probed with the valinomycin-K^+ complex. *Z. Naturforsch.* 47:757–761.

Snyder, S., D. Kim, and T. J. McIntosh. 1999. Lipopolysaccharide bilayer structure: effect of chemotype, core mutations, divalent cations, and temperature. *Biochemistry.* 38:10758–10767.

Texier, A. C., Y. Andres, M. Illemassene, and P. le Cloirec. 2000. Characterization of lanthanide ions binding sites in the cell wall of *Pseudomonas aeruginosa. Environ. Sci. Technol.* 34:610–615.

Texier, A. C., Y. Andres, and P. le Cloirec. 1999. Selective biosorption of lanthanide (La, Eu, Yb) ions by *Pseudomonas aeruginosa. Environ. Sci. Technol.* 33:489–495.

Truex, M. J., B. M. Peyton, N. B. Valentine, and Y. A. Gorby. 1997. Kinetics of U(VI) reduction by a dissimilatory Fe(III)-reducing bacterium under non-growth conditions. *Biotechnol. Bioeng.* 55:490–496.

Urrutia, M. M., E. E. Roden, and J. M. Zachara. 1999. Influence of aqueous and solid phase Fe(II) complexants on microbial reduction of crystalline iron(III) oxides. *Environ. Sci. Technol.* 33:4022–4028.

van Alten, D. M., J. B. C. de Groot, J. B. Findlay, H. J. Berendsen, and A. Amadei. 1997. A comparison of techniques for calculating protein essential dynamics. *J. Comp. Chem.* 18:169–181.

Wang, Y., and R. I. Hollingsworth. 1996. An NMR spectroscopy and molecular mechanics study of the molecular basis for the supramolecular structure of lipopolysaccharides. *Biochemistry.* 35:5647–5654.

Weber, W., H. Dermidjian, R. D. Lins, J. M. Briggs, R. Ferreira, and J. A. McCammon. 1998. Brownian and essential dynamics studies of the HIV-1 integrase catalytic domain. *J. Biomol. Struct. Dynam.* 16: 733–745.

Wiese, A., G. Schroder, K. Brandenburg, A. Hirsch., W. Welte, and U. Seydel. 1994. Influence of the lipid matrix on incorporation and function of LPS-free porin from *Paracoccus denitrificans. Biochim. Biophys. Acta.* 1190:231–242.

Woods, R. J., A. R. Dwek, and C. J. Edge. 1995. Molecular mechanical and molecular simulations of glycoproteins and oligosaccharides. 1. GLYCAM_93 parameter development. *J. Phys. Chem.* 99:3832–3846.